Application of a Laser Induced Fluorescence Model to the Numerical Simulation of Detonation Waves

Rémy Mével[1,2], **Dmitry Davidenko**[1], **Florian Pintgen**[3], **Joanna Austin**[4], **Joseph Shepherd**[2]

[1]ICARE-CNRS, Orléans, France
[2]California Institute of Technology, Pasadena, USA
[3]General Electric, Stamford, USA
[4]University of Illinois at Urbana-Champaign, Urbana, USA

1 Introduction

Austin et al. [1, 2] and Pintgen et al. [3, 4] performed simultaneous visualization of the shock front and the reaction zone in detonations using Schlieren and planar laser induced fluorescence (PLIF) techniques. These studies enable direct observation of the OH radical spatial distribution in the reaction zone. In weakly unstable detonations [4], the spatial distribution is characterized by alternative keystone-shaped features of high and low OH concentration created by the cellular structure of the detonation. In highly unstable detonations [2], other features such as shear layers, unreacted pockets, and fractal-like OH fronts are observed [5]. Although numerical simulations [6, 7] are able to qualitatively reproduce these geometric features, a direct comparison of the OH PLIF images has been carried out [8] only for one-dimensional segments using the ZND model as an approximation to the spatial structure normal to the front for weakly unstable waves.
In the present study, a 2-D detonation simulation is analyzed using a realistic but simplified model of the PLIF process. The detonation simulations are carried out using the unsteady, reactive, inviscid flow model with a detailed chemical reaction mechanism for H_2-O_2 mixtures. The resulting predictions of fluoresence intensity are compared with experimental results [1, 2] for weakly and moderately unstable cases with high argon and nitrogen dilution.

2 The Laser Induced Fluorescence model

Estimating the PLIF intensity behind a detonation front involves a number of physical processes that must be modeled in order to make quantitative estimates of flourescence emission. Pintgen [3, 8] was the first researcher successful in both obtaining PLIF images behind propagating detonation fronts, applying a model of the LIF process to detonations, and showing quantitative agreement between measured and modeled intensities. Based on Pintgen's results, Chapter 3 of [8], we adopt the simple 3-level model of Bessler et al. [9] to simulate the LIF process. Figure 1 shows a schematic representation of this model. The energy transfer processes considered are: stimulated absorption, stimulated emission, spontaneous emission, quenching, and rotational energy transfers. The rates of these processes are respectively referred to as b_{12}, b_{21}, A_{21} and A_{23i}, Q and R. In the framework of the 3-level model, the following assumptions are made to simplify the description of the LIF process: (i) the ground state rotational energy transfers are fast, (ii) the excited state rotational energy transfers are neglected, (iii) all allowed transitions between the excited state and the rovibrational levels of the ground state contribute to the fluorescence signal, and (iv) the photoionization and predissociation processes are neglected.

Correspondence to: mevel@cnrs-orleans.fr

In the linear regime, the LIF signal intensity, F, of a single pumped transition is obtained from the steady-state rate equation and is given by the following expression:

$$F \propto f_B \ \Gamma \ I_\nu^0 \ I_b \ N_{OH} \ B \ \frac{1}{Q} \ \sum \ A_i. \tag{1}$$

where the terms are: f_B: the Boltzmann fraction of OH radicals in the ground state; Γ: the dimensionless overlap integral; I_ν^0: the normalized spectral laser irradiance [J s/m]; I_b: a dimensionless factor accounting for the light sheet absorption; N_{OH}: the OH radical number density [m^{-3}]; B: the Einstein B coefficient [m^2/J s]; Q: the quenching rate [s^{-1}]; A_i: the Einstein A coefficients [s^{-1}].

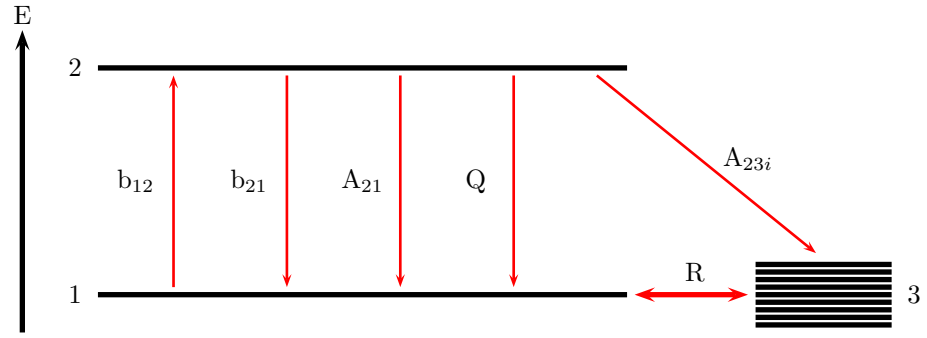

Figure 1: Schematic of the three energy level LIF model.

In the present study, the contributions of the $A^2\ \Sigma^+ \leftarrow X^2\ \Pi$ (1,0) Q2(8) and $A^2\ \Sigma^+ \leftarrow X^2\ \Pi$ (1,0) Q1(9) absorption lines, at 35210.25 and 35210.68 cm^{-1}, respectively, were taken into account. The LIF signal intensity was normalized with respect to the highest intensity value. The three level model of Figure 1 considers laser excitation from the ground state (1) to the upper state (2) and fluorescence emission due to transitions from (2) to all possible vibrational and rotational electronic ground states. A complete description of the LIF model can be found in [8]. A brief explanation is given below.

The Boltzmann fractions were determined using the partition function data from the HITRAN database [10]. The dimensionless overlap integral and the normalized spectral laser irradiance were calculated following the formulas given by Partridge and Laurendeau [11]. The laser line-shape was assumed to be Gaussian with a center line at ν_{0L}=35210.46 cm^{-1} (just in the middle between two absorption lines) and a full width at half maximum of $\Delta\nu_L$=0.1 cm^{-1}. The absorption line-shape function was obtained from the Doppler and the collision-broadened line-shape functions by using the modified pseudo-Voigt method proposed by Ida et al. [12]. This method provided a satisfactory accuracy and did not require computationally expensive fitting of the exact Voigt profile. The temperature dependence of the collisional broadening coefficient was described using the expression of Rea et al. [13]. The dimensionless factor accounting for the light sheet attenuation along its pass in the absorbing medium was directly obtained from the Beer-Lambert law. The absorbing species considered were H_2O and OH radicals (two absorption lines for OH). The collisional quenching rate of OH was calculated from the expression proposed by Paul [14]. The Einstein A and B coefficients were taken from the LIFBASE software database [15]. Finally, the OH concentration and the thermodynamic conditions were obtained from the ZND or 2-D detonation simulation.

3 Application to ZND simulation

In order to test the validity of the present LIF model and study the effect of some of its parameters, ZND solutions were post-processed and the simulated profiles of normalized intensity of the LIF signal were compared to the experimental results. The experimental data were extracted from the PLIF images. The experimental fluorescence intensity was averaged in the direction perpendicular to the laser propagation over 1 cm wide stripes oriented in the flow direction. The LIF intensity was then normalized with respect to the highest intensity value. This technique was first applied by Pintgen [8] to explain the observed features of the fluorescence signal behind the detonation front. The appearance of a sharp front is due to the exponential growth of OH (chain branching reactions) and the rapid decrease in intensity behind the front is due to the absorption of the excitation laser by the high concentration of OH in the combustion products.

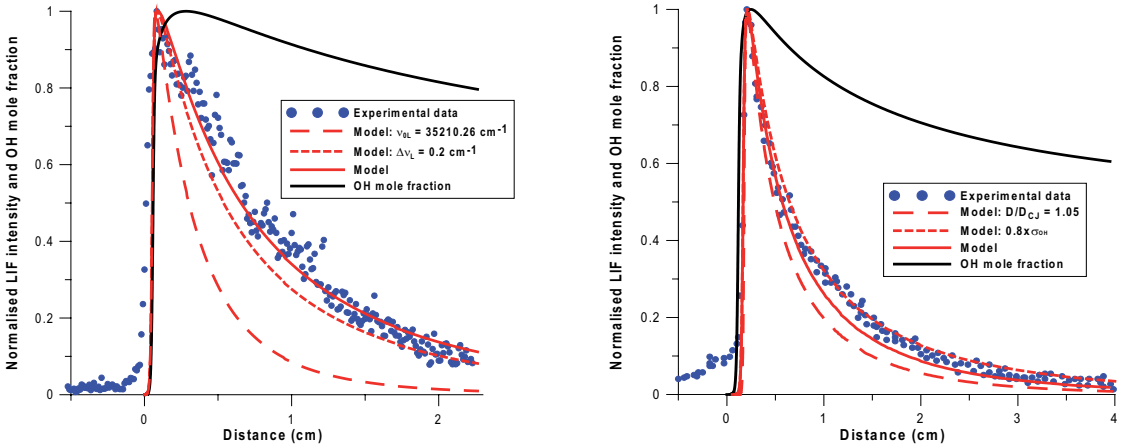

(a) (b)

Figure 2: Comparison of the experimental [1, 8] and calculated normalized LIF intensities for stoichiometric H_2-O_2 mixtures diluted with Ar and N_2. Initial conditions: a): $\Phi = 1$; $X_{Ar} = 0.8$; $T_1 = 295$ K ; $P_1 = 20$ kPa. b): $\Phi = 1$; $X_{N2} = 0.65$; $T_1 = 300$ K; $P_1 = 20$ kPa. Plain and dashed lines represent the base line and the perturbated model results, respectively.

Figure 2 presents some examples of the results obtained for detonations propagating in stoichiometric H_2-O_2-diluent mixtures. The kinetic model used was that of Mével [17]. It was validated for H_2-O_2 mixtures over a wide range of conditions including shock-tube, jet stirred and flow reactors, and laminar flame results. It can be seen that the agreement between the experimental and calculated LIF profiles is quite satisfactory. Both the rapid rise and the decrease of the LIF signal intensity is well reproduced by the model. The effect of the laser center line position and width are illustrated in Figure 2 (a). The model result with nominal parameters (given above) are shown as solid lines and model results with variations in the parameters are shown as dashed lines. The rate of decay of the LIF signal intensity with distance behind the peak is quite sensitive to both these parameters. The shift of the laser center line toward one of the two absorption lines or the increase of the laser line width both induce a faster decrease of the LIF signal. Figure 2 (b) illustrates the effects of the OH radical absorption cross section and the detonation velocity. The pertubated model results are shown as dashed lines. A decrease of the absorption cross section results in a noticeable reduction of the LIF intensity decay rate. If a slightly over-driven detonation (5% greater than CJ) is considered, the calculated LIF intensity decays only slightly faster than the CJ case. Also shown in Figure 2 are the normalized mole fractions of OH radicals. Comparing the LIF and OH mole fraction profiles, we see very clearly the dramatic effect of absorption of the light sheet propagating through the region of a high concentration of OH radicals in the combustion products.

4 Application to 2-D simulation

2-D simulations of detonations in a stoichiometric H_2-O_2 mixture with $X_{Ar} = 0.8$ and $X_{N2} = 0.6$ were performed using an Euler solver based on a Weighted Essentially Non-Oscillatory (WENO) scheme of the fifth order [16]. An automatic procedure has been used to obtain a reduced reaction model and rates starting from the kinetic model of Mével. Details about this procedure can be found in [17]. Error tolerances were the following: (i) 1% for the time to peak thermicity, (ii) 5% for the maximum thermicity, (iii) 20 K for the temperature profile and (iv) 1% for the molar mass profile. The reduction was performed for temperatures and pressures representative of a detonation propagating with a velocity ranging from 0.8 to 1.4 D_{CJ}. For the Ar diluted mixture, the reduced reaction model is composed of 17 reversible reactions and 9 species (including Ar). For the N_2 diluted mixture, the reduced reaction model is composed of 12 reversible reactions and 8 species. The pressure dependencies of the reaction rates are taken into account via the Lindeman and Troe formalisms. The computational mesh is structured with the finest resolution of 32 μm. Symmetry conditions were imposed on the upper and lower (perpendicular to the detonation propagation direction) boundaries. The width of the domain ranged from 13.6 to 20 mm.

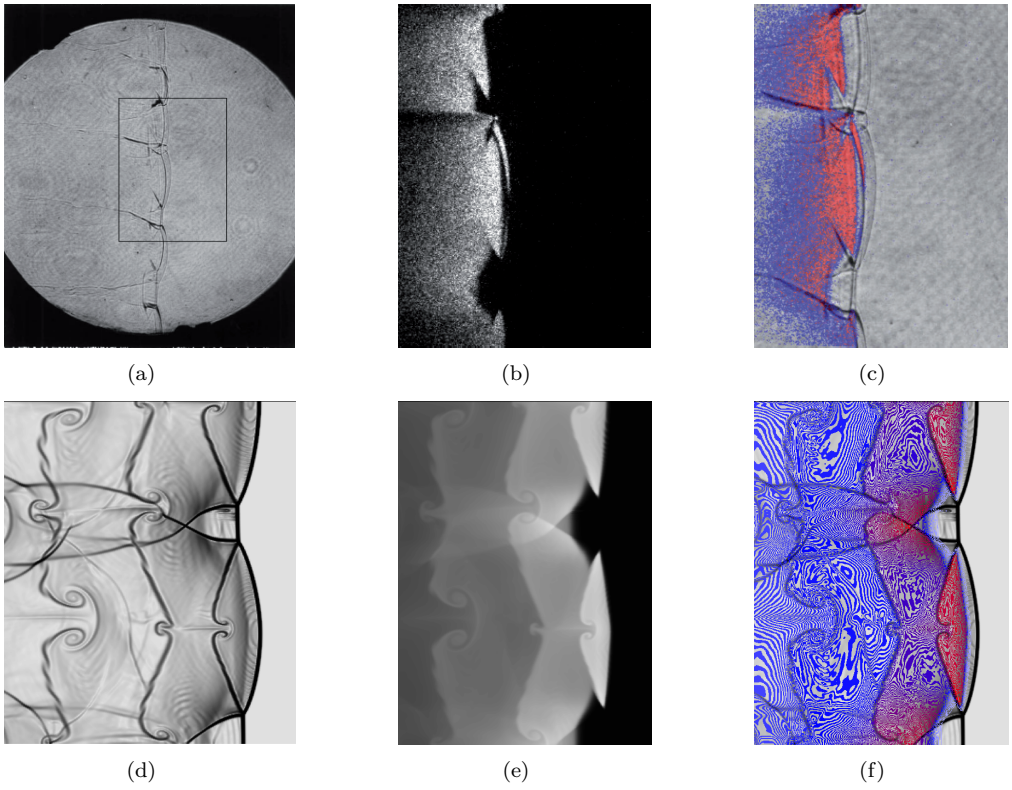

(a) (b) (c)

(d) (e) (f)

Figure 3: Comparison of experimental [1] (top) and numerical (bottom) images of a detonation wave propagating in a $2H_2$-O_2-12Ar mixture. Initial conditions: T_1=295 K and P_1=20 kPa. a), d): Schlieren images. b), e): OH PLIF images. c), f): superimposed Schlieren and PLIF images.

Figure 3 and Figure 4 compare the experimental and the numerical results. In each figure, Schlieren, PLIF and superimposed Schlieren-PLIF images are presented. Figure 3 has been obtained for an Ar diluted mixture, which is an example of a weakly unstable detonation with a reduced activation energy around 5, whereas Figure 4 has been obtained for a N_2 diluted mixture representing a moderately unstable detonation with a reduced activation energy around 6.5.

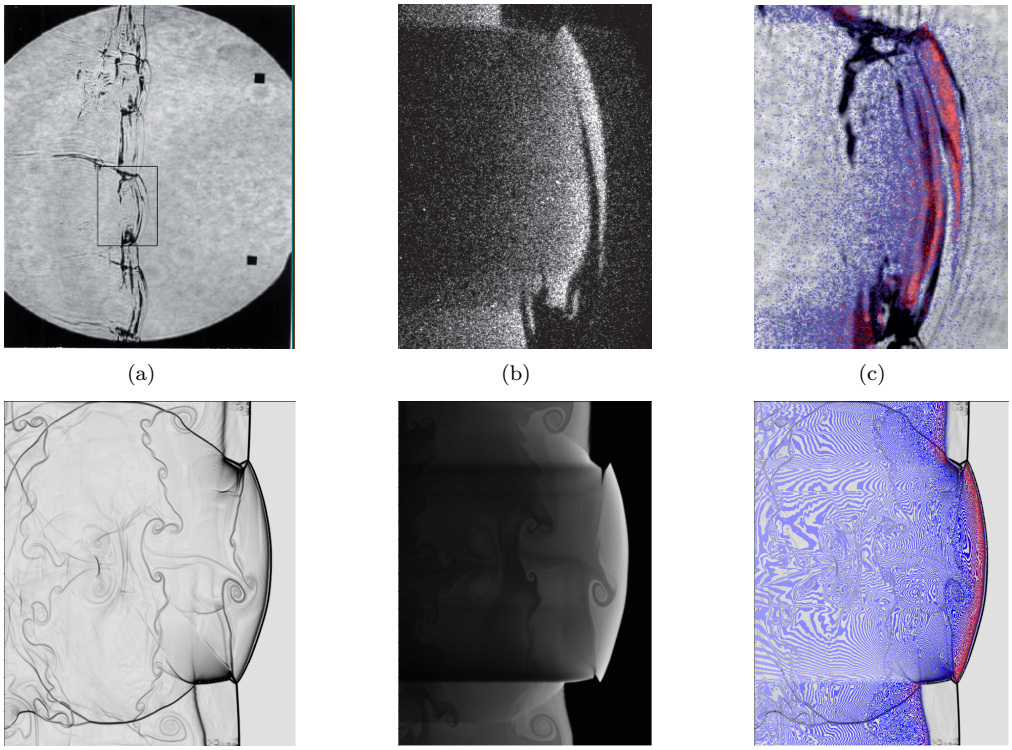

(a) (b) (c)

(d) (e) (f)

Figure 4: Comparison of experimental [1] (top) and numerical (bottom) images of a detonation wave propagating in a $2H_2$-O_2-$4.5N_2$ mixture. Initial conditions: T_1=295 K and P_1=20 kPa. a), d): Schlieren images. b), e): OH PLIF images. c), f): superimposed Schlieren and PLIF images.

For both cases, a reasonable agreement is observed for the overall features and many details for Schlieren, OH PLIF and superimposed images. The different instants of a cell cycle that can be seen on the experimental detonation images are well reproduced in the simulation. This indicates that the approach adopted in the present study allows qualitative description of the experimental phenomenon through-out a cell cycle. The observed spatial variations in the fluorescence image can clearly be directly linked to the varying OH concentrations created by the instability of the detonation front. In particular, the sharp onset and subsequent decay of the fluorescence signal are well predicted. The models also show that the vortex structures associated with Kelvin-Helmholtz instability of shear layer are indeed responsibile for the vortex-like flourescence images observed in the experiments [1, 2]. The progessive attenuation of the LIF signal intensity due to the laser sheet absorption is particularly apparent in the center of Figure 4, where a dark strip can be seen in the LIF images.
Despite the good qualitative agreement, it can be noted that some features of the experiment are not taken into account in the simulation. The experiments by Austin et al. [1, 2], have been performed in a 4.2 m long rectangular narrow channel. The channel section is 152 mm high and 18 mm wide. The detonation shock front and reaction zone are visualised through two large quartz windows located closed to the end of the narrow channel. As can be seen in Figure 3, the experimental detonation is not strictly 2-dimensional since two distinct fronts are observed in the Schlieren images. This feature can be explained by the presence of a single-mode out-of-plane instability which is not suppressed despite the narrow section of the experimental set-up [1]. Finally, despite the significant efforts made in both experiments and numerical simulation, further improvements can be made. Some simple improvements include accounting for the spatial distribution of the exciting laser sheet and the response characteristics

of the imaging camera. To go further will require substantial investment in technology and software development. Multi-wavelength techniques and careful accounting for processes such as quenching are needed in order to make the PLIF visualizations and analysis quantitative tools. Inclusion of molecular transport and three-dimensional motion is needed to obtain simulation results that can be quantitatively compared to the experiments.

5 Conclusion

In the present study, a laser induced fluorescence model has been applied for the first time to the results of detonation wave two-dimensional simulation. The sensitivity of the results to the parameters of the LIF model were examined by comparing one-dimensional slices of experimental data to simulated LIF signals based on ZND model solutions. These results show that a three-level LIF model with some simplifying assumptions can quantitatively reproduce the shape of the observed LIF signals. The LIF model was then applied to the output of two-dimensional, unsteady detonation simulations based on a detailed, but reduced reaction mechanism. Comparison of the predicted and observed LIF signals indicated that although the overall features of the observed LIF signals are well reproduced by the simulation, quantitative comparison is limited by a number of factors, particularly the three-dimensional nature of the experimental data.

References

[1] Austin J. (2003). Ph.D. thesis, California Institute of Technology.

[2] Austin J., Pintgen F. and Shepherd J. (2005). Proceedings of the Combustion Institute 30: 1849.

[3] Pintgen F. (2000). Master's thesis, Technische Universitt Mnchen and California Institute of Technology.

[4] Pintgen F. et al. (2003). Combustion and Flame 133: 211.

[5] Pintgen F. and Shepherd J.E. (2004). International colloquium on application of detonation for propulsion: 23.

[6] Khokhlov A. et al. (2004). 42^{th} AIAA Aerospace Sciences Meeting and Exhibit.

[7] Liang Z. et al. (2007). Proceedings of the Combustion Institute 31: 2445.

[8] Pintgen F. (2004). Ph.D. thesis, California Institute of Technology.

[9] Bessler G. et al. (2003). Third Joint Meeting of the U.S. Sections of The Combustion Institute.

[10] Rothman L. et al. (2003). Journal of Quantitative Spectroscopy and Radiative Transfer 82: 5.

[11] Partridge W. and Laurendeau N. (1995). Applied Optics 34: 2645.

[12] Ida T., Ando M. and Toraya H. (2000). Journal of Applied Crystallography 33: 1311.

[13] Rea E., Chang A. and Hanson R. (1987). Journal of Quantitative Spectroscopy and Radiative Transfer 37: 117.

[14] Paul P. (1994). Journal of Quantitative Spectroscopy and Radiative Transfer 51: 511.

[15] Luque J. and Crosley D. (1999). Technical report MP 99-009, SRI.

[16] Davidenko D., Mével R. and Dupré G. (in press). Shock Waves.

[17] Mével R. (2009). Ph.D. thesis, Université d'Orléans.